Editors' Suggestion   Featured in Physics

Precision Measurement of Reactor Antineutrino Oscillation at Kilometer-Scale Baselines by Daya Bay

F. P. An,[1] W. D. Bai,[1] A. B. Balantekin,[2] M. Bishai,[3] S. Blyth,[4] G. F. Cao,[5] J. Cao,[5] J. F. Chang,[5] Y. Chang,[6] H. S. Chen,[5] H. Y. Chen,[7] S. M. Chen,[7] Y. Chen,[8,1] Y. X. Chen,[9] Z. Y. Chen,[5] J. Cheng,[9] Z. K. Cheng,[1] J. J. Cherwinka,[2] M. C. Chu,[10] J. P. Cummings,[11] O. Dalager,[12] F. S. Deng,[13] Y. Y. Ding,[5] X. Y. Ding,[14] M. V. Diwan,[3] T. Dohnal,[15] D. Dolzhikov,[16] J. Dove,[17] H. Y. Duyang,[14] D. A. Dwyer,[18] J. P. Gallo,[19] M. Gonchar,[16] G. H. Gong,[7] H. Gong,[7] W. Q. Gu,[3] J. Y. Guo,[1] L. Guo,[7] X. H. Guo,[20] Y. H. Guo,[21] Z. Guo,[7] R. W. Hackenburg,[3] Y. Han,[1] S. Hans,[3,*] M. He,[5] K. M. Heeger,[22] Y. K. Heng,[5] Y. K. Hor,[1] Y. B. Hsiung,[4] B. Z. Hu,[4] J. R. Hu,[5] T. Hu,[5] Z. J. Hu,[1] H. X. Huang,[23] J. H. Huang,[5] X. T. Huang,[14] Y. B. Huang,[24] P. Huber,[25] D. E. Jaffe,[3] K. L. Jen,[26] X. L. Ji,[5] X. P. Ji,[3] R. A. Johnson,[27] D. Jones,[28] L. Kang,[29] S. H. Kettell,[3] S. Kohn,[30] M. Kramer,[18,30] T. J. Langford,[22] J. Lee,[18] J. H. C. Lee,[31] R. T. Lei,[29] R. Leitner,[15] J. K. C. Leung,[31] F. Li,[5] H. L. Li,[5] J. J. Li,[7] Q. J. Li,[5] R. H. Li,[5] S. Li,[29] S. C. Li,[25] W. D. Li,[5] X. N. Li,[5] X. Q. Li,[32] Y. F. Li,[5] Z. B. Li,[1] H. Liang,[13] C. J. Lin,[18] G. L. Lin,[26] S. Lin,[29] J. J. Ling,[1] J. M. Link,[25] L. Littenberg,[3] B. R. Littlejohn,[19] J. C. Liu,[5] J. L. Liu,[33] J. X. Liu,[5] C. Lu,[34] H. Q. Lu,[5] K. B. Luk,[30,18,35] B. Z. Ma,[14] X. B. Ma,[9] X. Y. Ma,[5] Y. Q. Ma,[5] R. C. Mandujano,[12] C. Marshall,[18,†] K. T. McDonald,[34] R. D. McKeown,[36,37] Y. Meng,[33] J. Napolitano,[28] D. Naumov,[16] E. Naumova,[16] T. M. T. Nguyen,[26] J. P. Ochoa-Ricoux,[12] A. Olshevskiy,[16] H.-R. Pan,[4] J. Park,[25] S. Patton,[18] J. C. Peng,[17] C. S. J. Pun,[31] F. Z. Qi,[5] M. Qi,[38] X. Qian,[3] N. Raper,[1] J. Ren,[23] C. Morales Reveco,[12] R. Rosero,[3] B. Roskovec,[15] X. C. Ruan,[23] B. Russell,[18] H. Steiner,[30,18] J. L. Sun,[39] T. Tmej,[15] K. Treskov,[16] W.-H. Tse,[10] C. E. Tull,[18] B. Viren,[3] V. Vorobel,[15] C. H. Wang,[6] J. Wang,[1] M. Wang,[14] N. Y. Wang,[20] R. G. Wang,[5] W. Wang,[1,37] X. Wang,[40] Y. Wang,[38] Y. F. Wang,[5] Z. Wang,[5] Z. Wang,[7] Z. M. Wang,[5] H. Y. Wei,[3,‡] L. H. Wei,[5] W. Wei,[14] L. J. Wen,[5] K. Whisnant,[41] C. G. White,[19] H. L. H. Wong,[30,18] E. Worcester,[3] D. R. Wu,[5] Q. Wu,[14] W. J. Wu,[5] D. M. Xia,[42] Z. Q. Xie,[5] Z. Z. Xing,[5] H. K. Xu,[5] J. L. Xu,[5] T. Xu,[7] T. Xue,[7] C. G. Yang,[5] L. Yang,[29] Y. Z. Yang,[7] H. F. Yao,[5] M. Ye,[5] M. Yeh,[3] B. L. Young,[41] H. Z. Yu,[1] Z. Y. Yu,[5] B. B. Yue,[1] V. Zavadskyi,[16] S. Zeng,[5] Y. Zeng,[1] L. Zhan,[5] C. Zhang,[3] F. Y. Zhang,[33] H. H. Zhang,[1] J. L. Zhang,[38] J. W. Zhang,[5] Q. M. Zhang,[21] S. Q. Zhang,[1] X. T. Zhang,[5] Y. M. Zhang,[1] Y. X. Zhang,[39] Y. Y. Zhang,[33] Z. J. Zhang,[29] Z. P. Zhang,[13] Z. Y. Zhang,[5] J. Zhao,[5] R. Z. Zhao,[5] L. Zhou,[5] H. L. Zhuang,[5] and J. H. Zou[5]

(Daya Bay Collaboration)

[1]*Sun Yat-Sen (Zhongshan) University, Guangzhou*
[2]*University of Wisconsin, Madison, Wisconsin 53706*
[3]*Brookhaven National Laboratory, Upton, New York 11973*
[4]*Department of Physics, National Taiwan University, Taipei*
[5]*Institute of High Energy Physics, Beijing*
[6]*National United University, Miao-Li*
[7]*Department of Engineering Physics, Tsinghua University, Beijing*
[8]*Shenzhen University, Shenzhen*
[9]*North China Electric Power University, Beijing*
[10]*Chinese University of Hong Kong, Hong Kong*
[11]*Siena College, Loudonville, New York 12211*
[12]*Department of Physics and Astronomy, University of California, Irvine, California 92697*
[13]*University of Science and Technology of China, Hefei*
[14]*Shandong University, Jinan*
[15]*Charles University, Faculty of Mathematics and Physics, Prague*
[16]*Joint Institute for Nuclear Research, Dubna, Moscow Region*
[17]*Department of Physics, University of Illinois at Urbana-Champaign, Urbana, Illinois 61801*
[18]*Lawrence Berkeley National Laboratory, Berkeley, California 94720*
[19]*Department of Physics, Illinois Institute of Technology, Chicago, Illinois 60616*
[20]*Beijing Normal University, Beijing*
[21]*Department of Nuclear Science and Technology, School of Energy and Power Engineering, Xi'an Jiaotong University, Xi'an*
[22]*Wright Laboratory and Department of Physics, Yale University, New Haven, Connecticut 06520*
[23]*China Institute of Atomic Energy, Beijing*
[24]*Guangxi University, No.100 Daxue East Road, Nanning*
[25]*Center for Neutrino Physics, Virginia Tech, Blacksburg, Virginia 24061*

^{26}Institute of Physics, National Chiao-Tung University, Hsinchu
^{27}Department of Physics, University of Cincinnati, Cincinnati, Ohio 45221
^{28}Department of Physics, College of Science and Technology, Temple University, Philadelphia, Pennsylvania 19122
^{29}Dongguan University of Technology, Dongguan
^{30}Department of Physics, University of California, Berkeley, California 94720
^{31}Department of Physics, The University of Hong Kong, Pokfulam, Hong Kong
^{32}School of Physics, Nankai University, Tianjin
^{33}Department of Physics and Astronomy, Shanghai Jiao Tong University,
Shanghai Laboratory for Particle Physics and Cosmology, Shanghai
^{34}Joseph Henry Laboratories, Princeton University, Princeton, New Jersey 08544
^{35}The Hong Kong University of Science and Technology, Clear Water Bay, Hong Kong
^{36}California Institute of Technology, Pasadena, California 91125
^{37}College of William and Mary, Williamsburg, Virginia 23187
^{38}Nanjing University, Nanjing
^{39}China General Nuclear Power Group, Shenzhen
^{40}College of Electronic Science and Engineering, National University of Defense Technology, Changsha
^{41}Iowa State University, Ames, Iowa 50011
^{42}Chongqing University, Chongqing

We present a new determination of the smallest neutrino mixing angle θ_{13} and the mass-squared difference Δm_{32}^2 using a final sample of 5.55×10^6 inverse beta-decay (IBD) candidates with the final-state neutron captured on gadolinium. This sample is selected from the complete dataset obtained by the Daya Bay reactor neutrino experiment in 3158 days of operation. Compared to the previous Daya Bay results, selection of IBD candidates has been optimized, energy calibration refined, and treatment of backgrounds further improved. The resulting oscillation parameters are $\sin^2 2\theta_{13} = 0.0851 \pm 0.0024$, $\Delta m_{32}^2 = (2.466 \pm 0.060) \times 10^{-3}$ eV^2 for the normal mass ordering or $\Delta m_{32}^2 = -(2.571 \pm 0.060) \times 10^{-3}$ eV^2 for the inverted mass ordering.

Neutrino oscillation has been firmly established by multiple observations since its discovery in 1998 [1]. As this phenomenon is not required by the Standard Model, it offers opportunities to search for new interactions and physical principles. The three-neutrino paradigm of neutrino oscillation can be parametrized by three mixing angles, two mass-squared differences, and a CP phase [2]. This framework has been very successful in explaining most of the observations made with accelerator, atmospheric, reactor and solar neutrinos. Our knowledge of the smallest neutrino mixing angle θ_{13} has been steadily improving since the first definitive determination in 2012 [3]. Besides being the best-measured neutrino mixing angle at present, precise knowledge of θ_{13} is important for testing the three-neutrino paradigm of neutrino mixing and as an invaluable input to model building and to other experiments, most notably in resolving the neutrino mass

hierarchy [4] and the search for CP violation in neutrino oscillation [5,6].

Nuclear reactors produce MeV-scale electron antineutrinos, $\bar{\nu}_e$s, that are ideal for determining θ_{13} and the mass-squared difference Δm_{32}^2 through the study of $\bar{\nu}_e$ disappearance. This is best accomplished by comparing the energy spectra obtained with identically designed detectors positioned at different distances from the reactors. This relative approach cancels the uncertainties in the absolute detection efficiency that are correlated between detectors and heavily suppresses the effect of the uncertainty in the reactor $\bar{\nu}_e$ flux determination, thus enabling precision measurement of the oscillation parameters. The $\bar{\nu}_e$s are detected via the inverse beta-decay reaction (IBD), $\bar{\nu}_e + p \rightarrow e^+ + n$, with the kinetic-energy loss and annihilation of the positron giving rise to a prompt-energy (E_p) signal, and the subsequent neutron capture to a delayed-energy (E_d) signal. The energy of the $\bar{\nu}_e$, $E_{\bar{\nu}_e}$, central to measurements of neutrino oscillation, is inferred from E_p with $E_{\bar{\nu}_e} \approx E_p + 0.78$ MeV.

In this Letter, we report a new measurement of $\sin^2 2\theta_{13}$ and Δm_{32}^2 using a final sample of 5.55×10^6 IBD candidates with the final-state neutron captured on gadolinium (n-Gd) acquired by the Daya Bay reactor neutrino experiment in 3158 days of operation.

We utilized up to eight antineutrino detectors (ADs) to detect $\bar{\nu}_e$s emitted from three pairs of 2.9-GW$_{\text{th}}$ reactors at the Daya Bay-Ling Ao nuclear power facility in Shenzhen, China. The ADs were installed in three underground experimental halls, EH1, EH2, and EH3, having a flux-averaged baseline of about 500, 500, and 1650 m from the reactors, respectively. To suppress ambient radiation, the ADs were submerged in water pools. Each pool was optically divided to function as inner (IWS) and outer (OWS) water Cherenkov detectors for detecting cosmic-ray muons. Four layers of resistive plate chambers (RPCs) covering the top of each water pool provided another independent muon detector. IBD events were detected with 20 tonnes of liquid scintillator doped with 0.1% gadolinium by weight (GdLS) in each AD [7–9]. The GdLS was contained in a 3-m-diameter acrylic cylinder enclosed inside a 4-m-diameter acrylic cylinder filled with 22 tonnes of undoped liquid scintillator (LS). Optical photons generated in the scintillator were detected with 192 photomultiplier tubes (PMTs) covering the barrel surface of the AD [10]. The PMTs were arranged in 8 horizontal rings and 24 vertical columns. Highly reflective disks sandwiching the 4-m acrylic vessel were used to enhance the detection efficiency of scintillation photons. Radioactive sources and LEDs were stored in three automatic calibration units (ACUs) on top of each AD [11,12]. Detailed information of the experiment can be found in Refs. [13,14]. For each AD, a cylindrical coordinate system with the vertical z axis being the symmetry axis and $z = 0$ at the AD center was used.

The Daya Bay experiment was operated with three different configurations of ADs in the three EHs. From 24 December 2011 to 28 July 2012 (217 days), the experiment ran in an initial six-AD configuration with 2 ADs in EH1, 1 AD in EH2, and 3 ADs in EH3 that resulted in the first observation of $\bar{\nu}_e$ disappearance at $\mathcal{O}(1\text{ km})$ baselines [3]. An AD was added to both EH2 and EH3 during the summer of 2012 and this eight-AD configuration was operated from 19 October 2012 until 20 December 2016 (1524 days). Seven-AD operation occurred from 26 January 2017 until 12 December 2020 (1417 days) with one AD in EH1 re-purposed for liquid scintillator R&D for the JUNO experiment [15].

The results presented in this Letter are based on the data collected in the three configurations. Throughout the entire data analysis process, multiple groups within the collaboration provided validation and cross-checks.

Details of the analysis process and techniques can be found in Refs. [16,17]. In this Letter, we focus on the improvements to the analysis techniques.

Accurate and precise measurement of the prompt energy E_p is essential for extracting the oscillation parameters from the spectra. After the gain of each PMT was calibrated with the single-photoelectron peak from dark noise, a correction for the nonlinear response of the electronics was applied to each channel. This correction was derived from the waveform output from a flash-ADC readout system running in parallel with the default ADC system of EH1-AD1 in 2016 [18]. The observed charge profile was then used to reconstruct the position of the event using reconstruction B in Ref. [16].

To obtain the reconstructed energy (E_{rec}), an additional correction to the nonuniform detector response was applied to account for a few nonfunctional PMTs toward the end of data collection. We used the energy deposited by spallation neutron capture on Gd in the GdLS and delayed α-particles from correlated decays of natural radioactivity, $^{214}\text{Bi} \rightarrow ^{214}\text{Po} \rightarrow ^{210}\text{Pb}$, in the LS to determine this additional position-dependent correction. The active volume of each AD was divided into 100 voxels in z and r^2, where r is the radial distance from the z axis. For each voxel, the correction was defined as the ratio of the reconstructed energy to the reconstructed energy averaged over the entire GdLS volume. The temporal dependence of this correction was accommodated by two calibration periods, before and after 31 March 2017. The largest additional per-voxel correction was about 3%.

In this Letter, the prompt energy was obtained by directly correcting E_{rec} for the nonlinear response of the LS which was determined from calibration [19]. Weekly calibration was performed by remotely lowering the calibration sources into the ADs from the ACUs. Specialized calibration runs were taken during the re-configuration periods [20]. The positron response model of Ref. [19] was updated, taking into account the measured responses of γ rays from various sources and electrons from β decay of cosmogenic ^{12}B of the full dataset as inputs. The best-fit model had a Birks' coefficient $k_B = 0.0143\text{ g/cm}^2/\text{MeV}$ for the quenching effect and $k_C = 0.023$ for the contribution of Cherenkov radiation to the nonlinearity; both parameters agreed well with the previous result [19]. The improved energy response model for the positron achieved a precision of $< 0.5\%$ for $E_p > 2\text{ MeV}$.

IBD candidates were selected with the following criteria. Events caused by spontaneous light emission of the PMTs, so-called flashers, were removed. Candidates must have a promptlike signal with $0.7\text{ MeV} < E_p < 12\text{ MeV}$ separated by 1 to 200 μs from a delayedlike signal with $6\text{ MeV} < E_d < 12\text{ MeV}$. Candidate pairs were vetoed if their delayedlike events occurred (i) within a $(-202\text{ μs}, 600\text{ μs})$ time window with respect to an IWS or OWS trigger [21] with a PMT-hit multiplicity (nHit) > 12, or (ii) within a $(-202\text{ μs}, 410\text{ μs})$ time window with respect to an IWS trigger with $6 < \text{nHit} \le 12$, or (iii) within a $(-202\text{ μs}, 1400\text{ μs})$ time window with respect to triggers in the same AD with energy between 20 MeV and 2 GeV or (iv) within a $(-202\text{ μs}, 0.4\text{ s})$ time window with respect to triggers in the same AD with energy higher than 2 GeV. This targeted muon veto efficiently removed spurious triggers that followed a muon as well as most muon-induced

spallation products and muon decays. To remove any ambiguity in the candidate-pair selection, no additional AD triggers with energy between 0.7 and 20 MeV were allowed within (-400 μs, 200 μs) of the delayed candidate.

A new source of flashers was observed in the 7-AD operation period that were not suppressed by the previous criteria [16]. Additional selection criteria targeting the characteristic charge pattern and temporal distribution of these new flashers were devised that rejected over 99% of this instrumental background with an IBD selection efficiency over 99.99%.

The selected IBD candidates consisted of genuine IBD and background events. The background comprised uncorrelated accidental pairs, and correlated prompt-and-delayed signals coming from fast neutrons, β-n decays of spallation ^{9}Li/^{8}He, neutrons leaking from the ^{241}Am-^{13}C calibration sources and ^{13}C$(\alpha, n)^{16}$O with the α coming from natural radioactivity. The latter two correlated backgrounds and the accidental background, detailed in Ref. [16], did not require any improved treatment in this analysis. The muon detection efficiency of the IWS and OWS dropped with time due to the gradual loss of functional PMTs near the top of the water pools, particularly in the 7-AD period. With this loss of detection efficiency, a new muon-induced background, compactly dubbed "muon-x" (described below), became apparent.

The largest correlated background is β-n decay of cosmogenic radioisotopes ^{9}Li and ^{8}He. To determine this background, muons were paired with all IBD candidates within ± 2 s. To improve discrimination of ^{9}Li/^{8}He from other processes, candidate events were separated into several samples based on the visible energy deposited by the muon (E_μ) in the AD and the distance between the prompt and delayed signals, Δr. The rates and energy spectra of the dominant cosmogenic radioisotopes were extracted with a simultaneous fit to 12 two-dimensional histograms defined by the different muon samples in the three experimental halls for the two Δr regions with a probability density function $\phi(E_p, \Delta t)$, where Δt is the time difference of the prompt-energy signal and the muon [22]. The distribution in Δt is described by a sum over radioisotopes, taking into account the known isotope lifetimes, and a term for uncorrelated muon-IBD pairs that is well constrained by the pairs in the region $\Delta t < 0$ s. Since the lifetimes of ^{9}Li and ^{8}He are comparable, we simply measured the sum of these two radioisotopes. The E_p distributions of the radioisotopes were determined from the fit. This method provides higher statistics and a better determination of the low-energy part of the β spectrum of ^{9}Li/^{8}He than the previous determination [16] while reducing the rate uncertainty to less than 25%.

We determined the combined contribution of the fast-neutron and muon-x processes to the background.

Energetic neutrons generated by cosmic-ray muon interactions in the vicinity of the water pool can enter the active volume of an AD. Proton recoil from neutron scattering in the LS and the subsequent neutron capture on gadolinium constituted the prompt and delayed signals of this fast-neutron background and dominates the correlated events with $E_p > 12$ MeV. The fast-neutron energy spectrum was determined from prompt signals in coincidence with muons detected only by the OWS or RPC within 0.5 μs of a prompt candidate with 0.7 MeV $< E_p < 250$ MeV. The measured spectra were similar in shape among the three experimental halls and stable throughout all three operational periods.

The muon-x background was caused by low-E_μ muons that passed through the IWS undetected. These events typically consisted of the muon as the prompt signal and a Michel electron from muon decay a product of muon capture or a spallation neutron as the delayed signal. Muon-x background was efficiently ($> 80\%$) suppressed by rejecting events with a delayed signal less than 410 μs after a muon identified with a more stringent IWS PMT-hit multiplicity requirement of $6 < $ nHit ≤ 12 which led to a $< 0.1\%$ loss in livetime.

To determine the rate of these two backgrounds, the prompt-energy spectrum above 12 MeV and the delayed-energy spectrum of the IBD-candidate sample with the prompt energy extended to 250 MeV were fitted to the spectra of the previously described fast-neutron sample and the muon-x sample with IWS nHit $= 7$. Their rates in the range of 0.7 MeV $< E_p < 12$ MeV were estimated by extrapolation. We found no muon-x background in the 6-AD period. In the 8-AD period, the rate of muon-x background was about 0.038 of that of the fast neutron in EH1, 0.0055 in EH2, and 0.023 in EH3. The ratios increased to 0.26, 0.15, and 0.53, respectively, in the 7-AD period, consistent with the reduction in the number of functional PMTs in the three IWSs. The combined systematic uncertainty of these two backgrounds was estimated to be about 20%, which is dominated by the fast neutron background.

Table I summarizes the IBD candidates and backgrounds for the final n-Gd sample. We obtained a total of 4.8×10^6 IBD candidates at the near halls and 0.76×10^6 at the far hall with less than 2% background.

The $\bar\nu_e$ flux without oscillation at each AD was predicted by using the thermal-power data and fission fractions of each fuel cycle, provided by the power plant operator, as a function of burn-up. The power data carried an uncorrelated uncertainty of 0.5% per core, while a 0.6% uncorrelated uncertainty per core in the $\bar\nu_e$ yield was introduced by the uncertainties of the fission fractions. Because of the nature of the near-far relative measurement, 95% of the uncorrelated uncertainty of each core cancelled and extraction of the oscillation parameters was insensitive to the spectral shape of the no-oscillation prediction.

The detector-related uncertainties have been presented in Ref. [16]. Detection efficiency uncertainties that are

TABLE I. Summary of IBD signal and background. Rates are corrected for the muon veto and multiplicity selection efficiencies $\varepsilon_\mu \times \varepsilon_m$. The sum of the fast neutron and muon-x background rates is reported as "Fast n + muon-x." The AD numbering scheme reflects the time order of AD fabrication and deployment. Uncertainties reported as 0.00 in the table are < 0.005 and nonzero.

	EH1		EH2		EH3			
	AD1	AD2	AD3	AD8	AD4	AD5	AD6	AD7
$\bar{\nu}_e$ candidates	794 335	144 247 5	132 830 1	121 659 3	194 949	195 369	193 334	180 762
DAQ live time [day]	1535.111	2686.110	2689.880	2502.816	2689.156	2689.156	2689.156	2501.531
$\varepsilon_\mu \times \varepsilon_m$	0.7743	0.7716	0.8127	0.8105	0.9513	0.9514	0.9512	0.9513
Accidentals [day^{-1}]	7.11 ± 0.01	6.76 ± 0.01	5.00 ± 0.00	4.85 ± 0.01	0.80 ± 0.00	0.77 ± 0.00	0.79 ± 0.00	0.66 ± 0.00
Fast n + muon-x [day^{-1}]	0.83 ± 0.17	0.96 ± 0.19	0.56 ± 0.11	0.56 ± 0.11	0.05 ± 0.01	0.05 ± 0.01	0.05 ± 0.01	0.05 ± 0.01
^{9}Li/^{8}He [AD^{-1} day^{-1}]	2.92 ± 0.78		2.45 ± 0.57		0.26 ± 0.04			
^{241}Am-^{13}C [day^{-1}]	0.16 ± 0.07	0.13 ± 0.06	0.12 ± 0.05	0.11 ± 0.05	0.04 ± 0.02	0.04 ± 0.02	0.04 ± 0.02	0.03 ± 0.01
^{13}C(α, n)^{16}O [day^{-1}]	0.08 ± 0.04	0.06 ± 0.03	0.04 ± 0.02	0.06 ± 0.03	0.04 ± 0.02	0.04 ± 0.02	0.03 ± 0.02	0.04 ± 0.02
$\bar{\nu}_e$ rate [day^{-1}]	657.2 ± 1.1	685.1 ± 1.0	599.5 ± 0.8	591.7 ± 0.8	75.0 ± 0.2	75.2 ± 0.2	74.4 ± 0.2	74.9 ± 0.2

correlated between detectors did not contribute to this near-far relative measurement. The total uncorrelated uncertainty in the detection efficiency remained at 0.13%. The largest contribution of 0.10% coming from the fraction of neutrons captured on gadolinium was obtained by comparing the capture-time distributions of the ADs. The next largest uncorrelated uncertainty of 0.08% in the delayed-energy selection criterion was due to a 0.2% spread in the relative energy scale among the ADs. The relative detection efficiency estimate was validated by comparing the $\bar{\nu}_e$ rates of neighboring ADs in each EH for each data-taking period [23]. The rates were consistent with the predictions that took the tiny variations in the baseline and number of protons into account. Furthermore, no significant deviation in the spectral distributions among the ADs in the same experimental hall was found.

We extracted the oscillation parameters using the survival probability of three-flavor oscillation given by

$$P = 1 - \cos^4\theta_{13}\sin^2 2\theta_{12}\sin^2\Delta_{21}$$
$$- \sin^2 2\theta_{13}(\cos^2\theta_{12}\sin^2\Delta_{31} + \sin^2\theta_{12}\sin^2\Delta_{32}), \quad (1)$$

where $\Delta_{ij} = \Delta m_{ij}^2 L/(4\hbar c E)$ with Δm_{ij}^2 in eV^2, L is the baseline in meters between an AD and a reactor core and E is the energy of the $\bar{\nu}_e$ in MeV. We used $\sin^2\theta_{12} = 0.307 \pm 0.013$ and $\Delta m_{21}^2 = (7.53 \pm 0.18) \times 10^{-5}$ eV^2 [2]. Alternatively, for short baselines of a few kilometers, the survival probability can be parametrized as

$$P = 1 - \cos^4\theta_{13}\sin^2 2\theta_{12}\sin^2\Delta_{21} - \sin^2 2\theta_{13}\sin^2\Delta_{ee}. \quad (2)$$

Here, the effective mass-squared difference Δm_{ee}^2 is related to the wavelength of the oscillation observed at Daya Bay, and is independent of the choice of neutrino mass ordering as well as the value and uncertainty of the mixing angle θ_{12} [16].

We adopted fitting method B reported in Ref. [16] to extract the oscillation parameters. The fit minimized a χ^2 function defined as [22]

$$\chi^2(\theta_{13}, \Delta m^2, \nu) = \chi_{\text{stat}}^2(\theta_{13}, \Delta m^2, \nu) + \chi_{\text{syst}}^2(\nu), \quad (3)$$

where χ_{stat}^2 is the standard statistical term that compares all the measured background-subtracted prompt-energy spectra with the predictions. For each period of operation, the spectrum of each AD was divided into 26 bins. The predictions were derived from the calculated reactor $\bar{\nu}_e$ flux, survival probability, IBD cross section [24], and detector response obtained with a detailed GEANT4-based simulation [25–27]. The term $\chi_{\text{syst}}^2(\nu)$ contains the detector and background systematic uncertainties as pulls of the nuisance parameters expressed as a vector ν.

Figure 1 shows the covariance contours in the $\Delta m_{ee}^2 - \sin^2 2\theta_{13}$ space. The best-fit point with $\chi^2/\text{ndf} = 559/517$
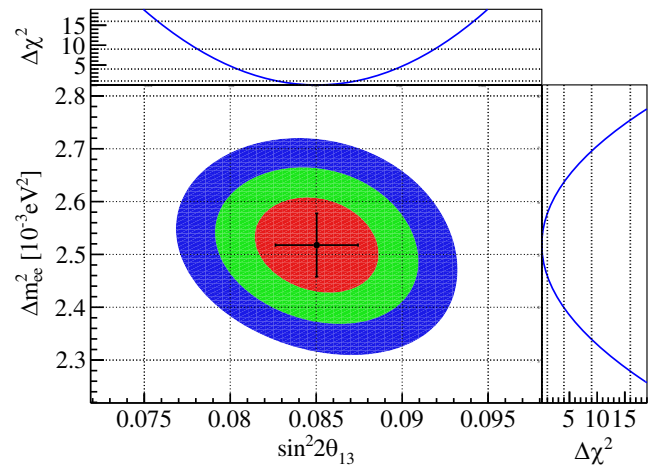

FIG. 1. Error ellipses in the Δm_{ee}^2-$\sin^2 2\theta_{13}$ space with the best-fit point indicated. The error bars display the one-dimensional 1-standard-deviation confidence intervals. The colored contours correspond to 1, 2, and 3 standard deviations. The $\Delta\chi^2$ distributions are also shown. These one-dimensional distributions were obtained by determining the smallest $\Delta\chi^2$ value after scanning through Δm_{ee}^2 ($\sin^2 2\theta_{13}$) for a given $\sin^2 2\theta_{13}$ (Δm_{ee}^2).
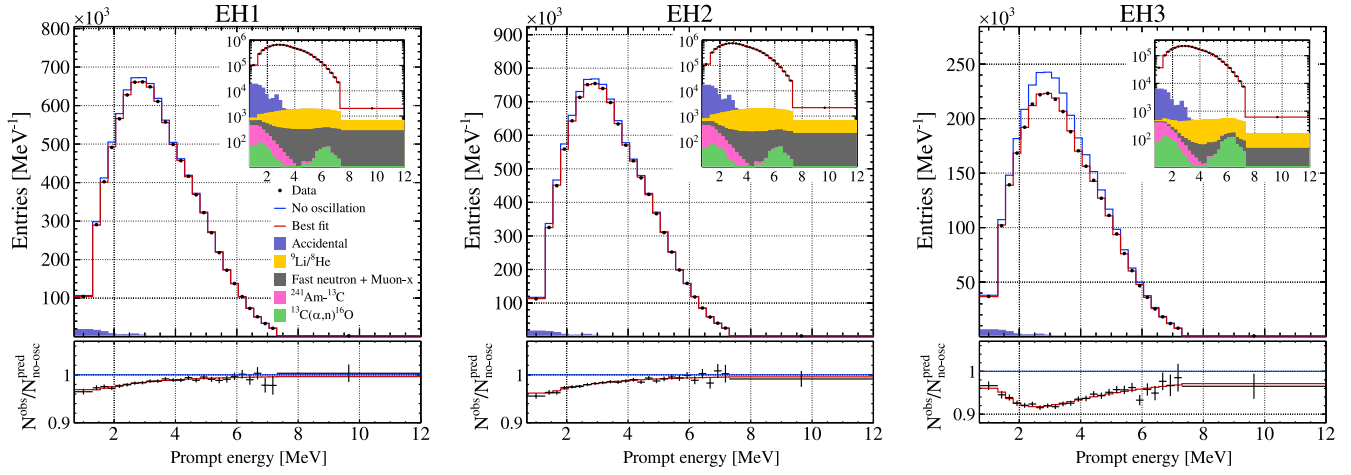
FIG. 2. The measured prompt-energy spectra of EH1, EH2, and EH3 with the best-fit and no-oscillation curves superimposed in the upper panels. The shape of the backgrounds are apparent in the spectra with a logarithmic ordinate shown in the insets. The backgrounds shown in the legend are in descending order according to their contribution. The lower panels shows the ratio of the observed spectrum to the predicted no-oscillation distribution. The error bars are statistical.

yields $\sin^2 2\theta_{13} = 0.0851 \pm 0.0024$, and $\Delta m^2_{32} = (2.466 \pm 0.060) \times 10^{-3}$ eV^2 for the normal mass hierarchy or $\Delta m^2_{32} = -(2.571 \pm 0.060) \times 10^{-3}$ eV^2 for the inverted mass hierarchy. Using Eq. (2), we obtained $\sin^2 2\theta_{13} = 0.0852 \pm 0.0024$ and $\Delta m^2_{ee} = (2.519 \pm 0.060) \times 10^{-3}$ eV^2 with the same reduced-χ^2 value. Results determined with the other fitting methods described in Ref. [16] were consistent to < 0.2 standard deviations.

The best-fit prompt-energy distribution is in excellent agreement with the observed spectra in each experimental hall, as shown in Fig. 2.

Figure 3 depicts the normalized signal rate of the three halls as a function of $L_{\text{eff}}/\langle E_{\bar{\nu}_e}\rangle$ with the best-fit curve superimposed, where L_{eff} and $\langle E_{\bar{\nu}_e}\rangle$ are the effective
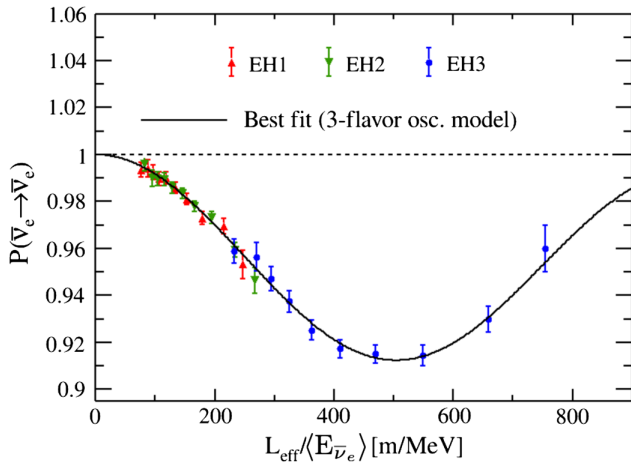

FIG. 3. Measured disappearance probability as a function of the ratio of the effective baseline L_{eff} to the mean antineutrino energy $\langle E_{\bar{\nu}_e}\rangle$.

baseline and average $\bar{\nu}_e$ energy, respectively [16]. The oscillation pattern related to θ_{13} is unambiguous.

The present improved result in $\sin^2 2\theta_{13}$ is consistent with our previous determinations [3,16,17] and agrees with other measurements of reactor $\bar{\nu}_e$ disappearance by RENO [28] and Double Chooz [29,30] as well as electron neutrino and antineutrino appearance measurements by T2K [6]. Daya Bay's measured Δm^2_{32} is consistent with the results of NOvA [5], T2K [6], MINOS/MINOS+ [31], IceCube [32], and SuperK [33] that were obtained with muon (anti) neutrino disappearance. The agreement in $\sin^2 2\theta_{13}$ and Δm^2_{32} between Daya Bay measurements using $\bar{\nu}_e$ and the muon neutrino and antineutrino determinations provides strong support of the three-neutrino paradigm.

To conclude, we have presented a new determination of $\sin^2 2\theta_{13}$ with a precision of 2.8% and the mass-squared differences reaching a precision of about 2.4%. The reported $\sin^2 2\theta_{13}$ will likely remain the most precise measurement of θ_{13} in the foreseeable future and be crucial to the investigation of the mass hierarchy and CP violation in neutrino oscillation [34,35].

---

*Present address: Department of Chemistry and Chemical Technology, Bronx Community College, Bronx, New York 10453, USA.

†Present address: Department of Physics and Astronomy, University of Rochester, Rochester, New York 14627, USA.

‡Present address: Department of Physics and Astronomy, Louisiana State University, Baton Rouge, Louisiana 70803, USA.

[1] Y. Fukuda *et al.* (Super-Kamiokande Collaboration), Phys. Rev. Lett. **81**, 1562 (1998).

[2] P. A. Zyla *et al.* (Particle Data Group), Prog. Theor. Exp. Phys. **2020**, 083C01 (2020).

[3] F. P. An *et al.* (Daya Bay Collaboration), Phys. Rev. Lett. **108**, 171803 (2012).

[4] A. Abusleme *et al.* (JUNO Collaboration), Prog. Part. Nucl. Phys. **123**, 103927 (2022).

[5] M. A. Acero *et al.* (NOvA Collaboration), Phys. Rev. Lett. **123**, 151803 (2019).

[6] K. Abe *et al.* (T2K Collaboration), Phys. Rev. D **103**, 112008 (2021).

[7] M. Yeh, A. Garnov, and R. L. Hahn, Nucl. Instrum. Methods Phys. Res., Sect. A **578**, 329 (2007).

[8] Y. Y. Ding, Z. Y. Zhang, J. C. Liu, Z. M. Wang, P. J. Zhou, and Y. L. Zhao, Nucl. Instrum. Methods Phys. Res., Sect. A **584**, 238 (2008).

[9] W. Beriguete *et al.*, Nucl. Instrum. Methods Phys. Res., Sect. A **763**, 82 (2014).

[10] K. Chow *et al.* (Daya Bay Collaboration), Nucl. Instrum. Methods Phys. Res., Sect. A **794**, 25 (2015).

[11] J. Liu *et al.*, Nucl. Instrum. Methods Phys. Res., Sect. A **750**, 19 (2014).

[12] J. Liu, R. Carr, D. A. Dwyer, W. Q. Gu, G. S. Li, R. D. McKeown, X. Qian, R. H. M. Tsang, F. F. Wu, and C. Zhang, Nucl. Instrum. Methods Phys. Res., Sect. A **797**, 260 (2015).

[13] F. P. An *et al.* (Daya Bay Collaboration), Nucl. Instrum. Methods Phys. Res., Sect. A **773**, 8 (2015).

[14] F. P. An *et al.* (Daya Bay Collaboration), Nucl. Instrum. Methods Phys. Res., Sect. A **811**, 133 (2016).

[15] A. Abusleme *et al.* (JUNO and Daya Bay Collaborations), Nucl. Instrum. Methods Phys. Res., Sect. A **988**, 164823 (2021).

[16] F. P. An *et al.* (Daya Bay Collaboration), Phys. Rev. D **95**, 072006 (2017).

[17] D. Adey *et al.* (Daya Bay Collaboration), Phys. Rev. Lett. **121**, 241805 (2018).

[18] Y. B. Huang *et al.*, Nucl. Instrum. Methods Phys. Res., Sect. A **895**, 48 (2018).

[19] D. Adey *et al.* (Daya Bay Collaboration), Nucl. Instrum. Methods Phys. Res., Sect. A **940**, 230 (2019).

[20] H. X. Huang *et al.*, J. Instrum. **8**, P09013 (2013).

[21] An IWS trigger required a PMT-hit multiplicity of > 6. A near(far) hall OWS trigger required a PMT-hit multiplicity of > 7 (> 8).

[22] See Supplemental Material at http://link.aps.org/supplemental/10.1103/PhysRevLett.130.161802 for the χ^2 expressions used for determining the fast-neutron and muon-x backgrounds and for extracting $\sin^2 2\theta_{13}$ and Δm_{ee}^2, the observed prompt-energy spectra for the inverse decay candidates and estimated backgrounds for each experimental hall, and the distribution of $\Delta\chi^2$ as a function of $\sin^2 2\theta_{13}$ and Δm_{ee}^2.

[23] F. P. An *et al.* (Daya Bay Collaboration), Nucl. Instrum. Methods Phys. Res., Sect. A **685**, 78 (2012).

[24] P. Vogel and J. F. Beacom, Phys. Rev. D **60**, 053003 (1999).

[25] S. Agostinelli *et al.*, Nucl. Instrum. Methods Phys. Res., Sect. A **506**, 250 (2003).

[26] J. Allison *et al.*, IEEE Trans. Nucl. Sci. **53**, 270 (2006).

[27] J. Allison *et al.*, Nucl. Instrum. Methods Phys. Res., Sect. A **835**, 186 (2016).

[28] G. Bak *et al.* (RENO Collaboration), Phys. Rev. Lett. **121**, 201801 (2018).

[29] H. de Kerret *et al.* (Double Chooz Collaboration), Nat. Phys. **16**, 558 (2020).

[30] T. Abrahão *et al.* (Double Chooz Collaboration), J. High Energy Phys. 01 (2021) 190.

[31] P. Adamson *et al.* (MINOS+Collaboration), Phys. Rev. Lett. **125**, 131802 (2020).

[32] M. G. Aartsen *et al.* (IceCube Collaboration), Phys. Rev. Lett. **120**, 071801 (2018).

[33] K. Abe *et al.* (Super-Kamiokande Collaboration), Phys. Rev. D **97**, 072001 (2018).

[34] R. Acciarri *et al.* (DUNE Collaboration), arXiv:1512.06148.

[35] K. Abe *et al.* (Hyper-Kamiokande Collaboration), arXiv:1109.3262.